catalysts

MDPI

Review

Recent Progress in Electrocatalytic CO_2 Reduction to Pure Formic Acid Using a Solid-State Electrolyte Device

Yeomin Kang, Taekyung Kim, Koo Young Jung and Ki Tae Park *

Department of Chemical Engineering, Konkuk University, 120 Neungdong-ro, Gwangjin-gu, Seoul 05029, Republic of Korea; yestink@konkuk.ac.kr (Y.K.); fkschakt1004@konkuk.ac.kr (T.K.); marino0303@konkuk.ac.kr (K.Y.J.)

* Correspondence: kpark@konkuk.ac.kr

Abstract: The electrocatalytic CO_2 reduction reaction (CO_2RR) to formic acid has gained significant attention as a potential environmentally friendly approach to reducing CO_2 emissions and producing carbon-neutral liquid fuels. However, several challenges must be addressed to achieve the production of high-purity and high-concentration formic acid through CO_2RR. One major challenge is the formation of a formate mixture instead of pure formic acid in conventional reactors. This requires costly downstream purification and concentration processes to obtain pure formic acid. To overcome this problem, a three-compartment reactor design has been proposed where a solid-state electrolyte (SSE) is inserted between the anode and cathode compartments to recover pure formic acid directly. This reactor design involves the use of an anion exchange membrane (AEM) and a cation exchange membrane (CEM) to separate the anode and cathode compartments, and a center compartment filled with high-conductivity SSE to minimize ohmic resistance. Several studies have implemented this reactor design for continuous CO_2RR and have reported remarkable improvements in the concentration and purity of the formic acid product. In this review, we summarize the recent progress of the SSE reactor design for CO_2RR to produce pure formic acid (HCOOH) and propose further research to scale up this technology for industrial-scale applications in the future.

Keywords: carbon dioxide; CO_2 electroreduction; formate; formic acid; solid-state electrolyte

check for updates

Citation: Kang, Y.; Kim, T.; Jung, K.Y.; Park, K.T. Recent Progress in Electrocatalytic CO_2 Reduction to Pure Formic Acid Using a Solid-State Electrolyte Device. *Catalysts* **2023**, *13*, 955. https://doi.org/10.3390/catal13060955

Academic Editor: Ali Seifitokaldani

Received: 28 April 2023
Revised: 22 May 2023
Accepted: 30 May 2023
Published: 31 May 2023

1. Introduction

Anthropogenic activities, particularly the excessive usage of fossil fuels, have led to a significant increase in the level of CO_2 in the atmosphere since the beginning of the industrial period [1]. This rise in CO_2 levels has contributed to a climate crisis, evident from the recent occurrence of extreme weather events such as floods and forest fires. To address these challenges and reduce greenhouse gas emissions, substantial efforts have been directed toward finding ways to convert CO_2 into value-added chemicals or fuels, including methanol (CH_3OH), formate ($HCOO^-$)/formic acid (HCOOH), carbon monoxide (CO), syngas (CO and H_2), and ethylene (C_2H_4) [2]. Among the numerous CO_2 conversion approaches such as biochemical, thermochemical, photochemical, and electrochemical methods, electrocatalytic CO_2 reduction reaction (CO_2RR) is attracting significant attention as an environmentally friendly approach. CO_2RR can be coupled with intermittent renewable energies due to its mild operating conditions with room temperature and atmospheric pressure. It enables the conversion of CO_2 into value-added products without additional emissions (Figure 1) [3–6]. Due to their high selectivity (>90%) and activity (>100 mA cm^{-2}) for industrial applications, the cost of certain CO_2RR products, particularly C_1 chemicals such as CO and formic acid, has become economically competitive with traditional chemical processes [7–12]. This trend has been further supported by the decreasing price of renewable electricity.

Liquid products such as $HCOO^-$/HCOOH offer significant advantages over gas-phase CO_2RR products due to their high energy densities and ease of storage and distribution [13,14]. Formic acid, in particular, is a crucial chemical feedstock with a global production of approximately 800,000 metric tons per year, used in a wide range of applications, including chemical production, cleaning, the textile industry, and antiseptics [15–18]. Moreover, formic acid has gained attention as a promising hydrogen carrier due to its high volumetric hydrogen density (53 g H_2 per liter of HCOOH), low toxicity, and the fact that it is in the liquid phase under ambient conditions [19,20]. It is also considered an energy carrier for fuel cell applications due to its stability, low volatility, and high volumetric capacity [21,22]. Thus, producing formic acid through electrochemical CO_2RR can serve as a carbon-neutral liquid fuel, effectively offsetting carbon emissions [23]. However, several challenges must be addressed for the practical applications of CO_2RR in renewable formic acid production: (i) improving the selectivity, activity, and durability of the catalysts; (ii) reducing the energy consumption and cost of the process; (iii) scaling up the technology and integrating it with renewable energy sources; (iv) separating the product from aqueous mixture. Additional purification steps are often required, increasing production costs [23–26].

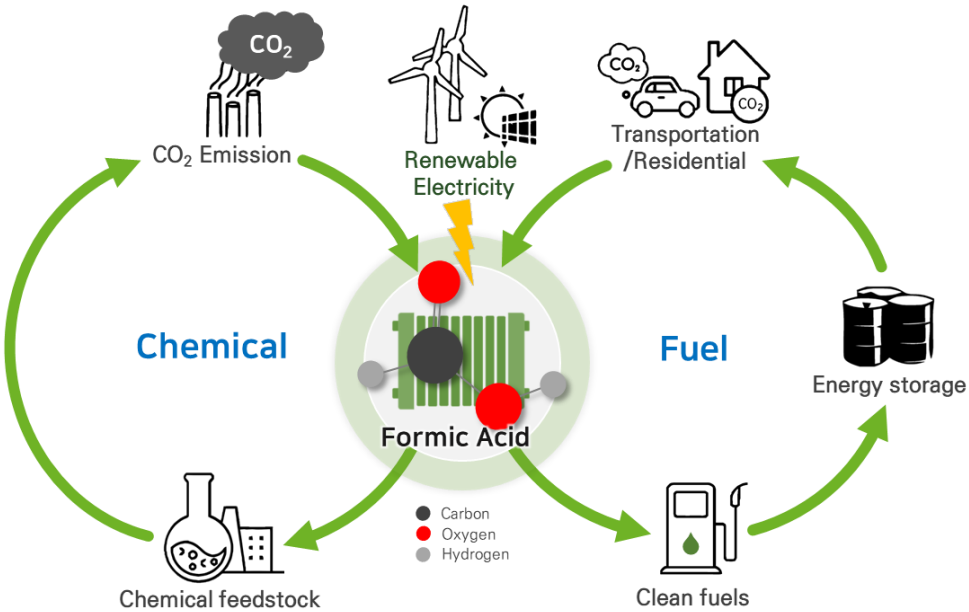

Figure 1. Carbon-neutral cycles of produced formic acid via CO_2RR using renewable electricity.

To address the limitations in CO_2RR for formic acid production, extensive research efforts have been focused on developing efficient electrocatalysts, suitable electrolytes, and reactor designs to achieve high productivity. In particular, catalyst development has received significant attention to improving the selectivity and activity toward $HCOO^-$/HCOOH production. Recent studies have made notable progress in identifying and designing efficient electrocatalysts for the selective production of $HCOO^-$/HCOOH. For example, studies on the development of nanostructured and bimetallic catalysts have shown promising results in achieving high selectivity and activity for CO_2RR to $HCOO^-$/HCOOH [27–36]. In addition, single-atom catalysts (SACs) for CO_2RR to $HCOO^-$/HCOOH have been investigated due to their high surface area and atomic-level dispersion of active sites, which can enhance their electrocatalytic performance [12].

Nevertheless, there are other practical challenges that require technological advancements beyond the scope of electrocatalyst design. One prominent challenge is the purity and concentration of the liquid products [37]. In recent years, research efforts have been focused on developing efficient and scalable reactors for CO_2RR to formate/formic acid with a growing demand for technologies and devices that enable direct formic acid pro-

duction. One promising approach is the use of an additional compartment of solid-state electrolyte (SSE) inserted between the anode and cathode compartments [23,26,38,39]. In this reactor design, the cathode and anode are in contact with an anion exchange membrane (AEM) and a cation exchange membrane (CEM), respectively. The $HCOO^-$ and H^+ ions generated at the cathode and anode migrate across the AEM and CEM, respectively, into the center compartment, in which pure HCOOH molecules are formed via ionic recombination. In this review, we emphasize the significance and challenges associated with the direct production of high-purity formic acid by reviewing the recent progress of SSE devices for CO_2RR and discussing strategies to enhance selectivity, activity, and purity for the direct production of pure formic acid. This work provides valuable insights and guidelines for the design of electrolyzers capable of producing pure liquid fuels through CO_2RR, bringing us closer to large-scale applications in the future.

2. Electrocatalytic CO_2 Reduction to Formate

2.1. CO_2RR to Formate Using CO_2-Dissolved Liquid Feed

In early CO_2RR studies, numerous research groups have utilized reactors such as 3-electrode and H-type cells to produce formate in aqueous solutions. Figure 2 illustrates the typical configuration of an H-type cell, where the cathode and anode chambers are separated by an ion exchange membrane. This type of reactor has been widely employed for investigating various CO_2RR catalysts due to its versatile setup. In these experiments, the catholyte is saturated with CO_2 by continuous bubbling using a glass sparger before electrolysis. The CO_2 gas is supplied continuously to the catholyte throughout the experiment to improve the absorption of the CO_2 gas in the aqueous solution [27]. Researchers have utilized this reactor configuration to develop highly active and selective electrocatalysts for CO_2RR [27,29–36,40]. Since the previous works by Hori et al. described the classification of metal catalysts according to product selectivity for CO_2RR [41], extensive efforts have been made to develop various heterogeneous metal-based catalysts for selective CO_2RR to formate. Table 1 summarizes some of the metal catalysts that have been investigated for their potential in CO_2RR to formate, including tin (Sn), lead (Pb), bismuth (Bi), and indium (In).

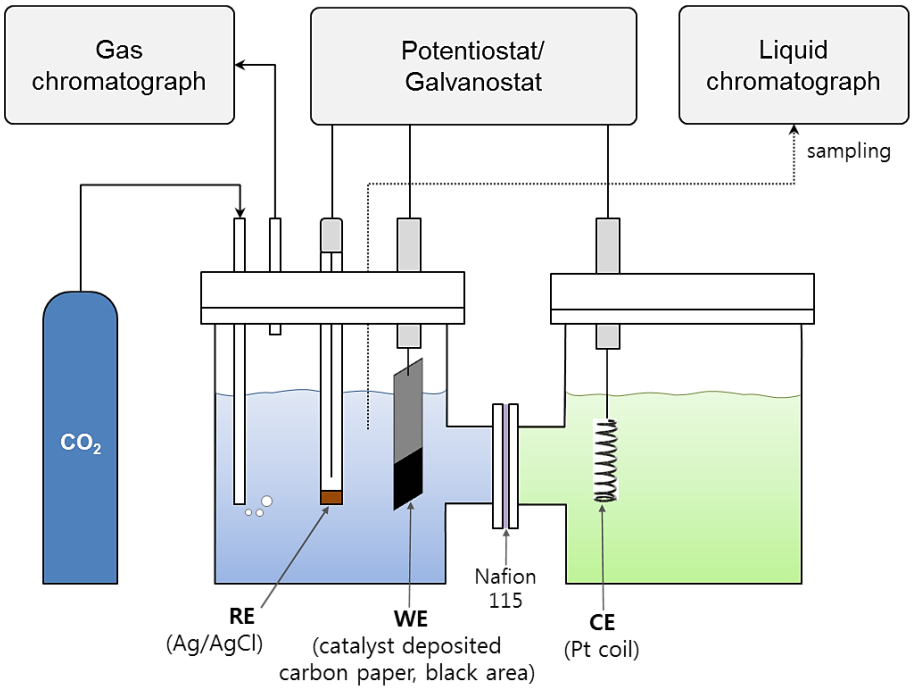

Figure 2. Schematic diagram of the electrocatalytic CO_2 reduction (CO_2RR) to formate in an H-type cell reaction system (Reprinted with permission from reference [27]. Copyright 2016 American Chemical Society).

Table 1. Figures of merits of studies reported in the literature for the CO_2RR to formate in terms of reactor type, catalysts of the cathode, electrolytes (for 3-electrode cell) or catholyte (for H-type cell), applied potential (vs. reference electrode), faradaic efficiency, and current density for formate production.

Reactor Type	Cathode	Electrolyte (Catholyte)	Potential (V vs. RHE)	$FE_{formate}$ (%)	$j_{formate}$ (mA cm^{-2})	Reference
3-electrode	Sn/SnO_2 porous hollow fiber	0.1 M $KHCO_3$	−0.95	82.1	22.9	[32]
	Bi on Cu foil	0.5 M $KHCO_3$	−0.86	91.3	3.08	[33]
	Bi-Sn	0.1 M $KHCO_3$	−1.0	93.9	9.3	[34]
H-type	Sn-Pb alloy	0.5 M $KHCO_3$	−1.36	79.8	45.7	[27]
	SnO_2/ZnO hollow nanofiber	0.1 M $KHCO_3$	−1.34	97.9	24.9	[29]
	Pd-Sn alloy/C	0.5 M $KHCO_3$	−0.43	99.6	~2	[35]
	Mesoporous SnO_2	0.1 M $KHCO_3$	−1.15	75	10.8	[40]
	$In_{16}Bi_{84}$ nano-sphere	0.5 M $KHCO_3$	−0.94	100	14.08	[30]
	AgSn/SnOx (core-shell)	0.5 M $KHCO_3$	−0.8	80	16	[36]
	In-doped SnO_2 nanowires	0.5 M $KHCO_3$	−1.04	82	6.02	[31]

Choi et al. studied the CO_2RR to formate in an aqueous solution using tin–lead (Sn–Pb) alloys [27]. The study found that the $Sn_{56.3}Pb_{43.7}$ alloy exhibits high faradaic efficiency ($FE_{formate}$ of 79.8%) and current density ($j_{formate}$ of 45.7 mA cm^{-2}) for formate synthesis; 16%, and 25% improved $FE_{formate}$ and $j_{formate}$ compared to the single metal electrodes (Figure 3).

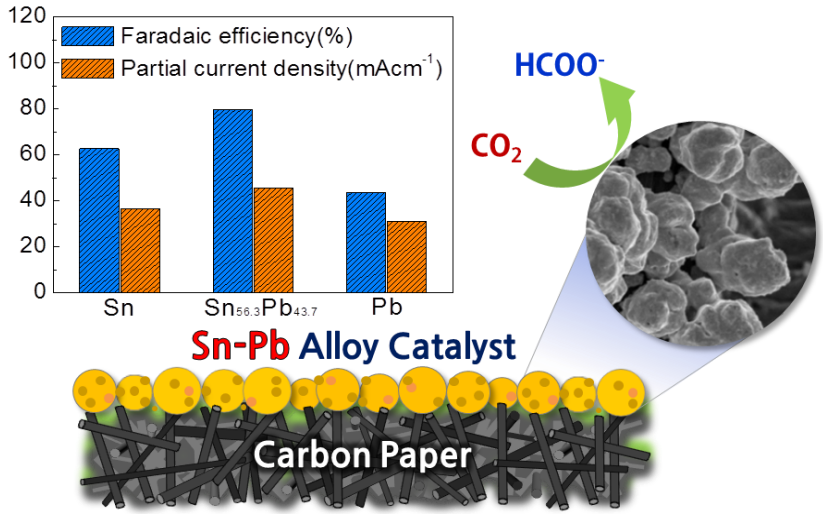

Figure 3. The faradaic efficiency and current density of formate generation on the Sn–Pb alloys in an H-type cell at −1.36 V (vs. RHE) compared with Sn and Pb (Reprinted with permission from reference [27]. Copyright 2016 American Chemical Society).

Tan et al. reported a highly efficient CO_2RR to formate on a tin (IV) oxide/zinc oxide (SnO_2/ZnO) composite electrocatalyst with a grainy hollow nanofiber (HNF) structure [29]. The faradaic efficiency (FE) of formate on the SnO_2/ZnO composite HNF reaches as high as 97.9% at −1.34 V (vs. RHE), outperforming many Sn-based catalysts. At −1.54 V (vs. RHE), the SnO_2/ZnO HNF exhibits 2 times and 4 times higher current density for formate generation than those of SnO_2 HNF and nanoparticles (NPs), respectively. This superior catalytic performance is attributed to its one-dimensional continuous structure as well as to the synergistic effects between SnO_2 and ZnO, which facilitate faster electron transfer and improve the conductivity of SnO_2/ZnO composite HNF (Figure 4).

Despite these significant results, the kinetics of CO_2RR into formate is limited below 50 mA cm^{-2} (Table 1) due to the polarization losses caused by the low solubility of CO_2 in the electrolyte, and the mass transfer limitation of OH^- near the electrodes, inevitably

limiting the productivity of CO_2RR [42]. In particular, the low solubility of CO_2 in the aqueous catholyte significantly limits the current density, thus hindering the large-scale application of the CO_2RR.

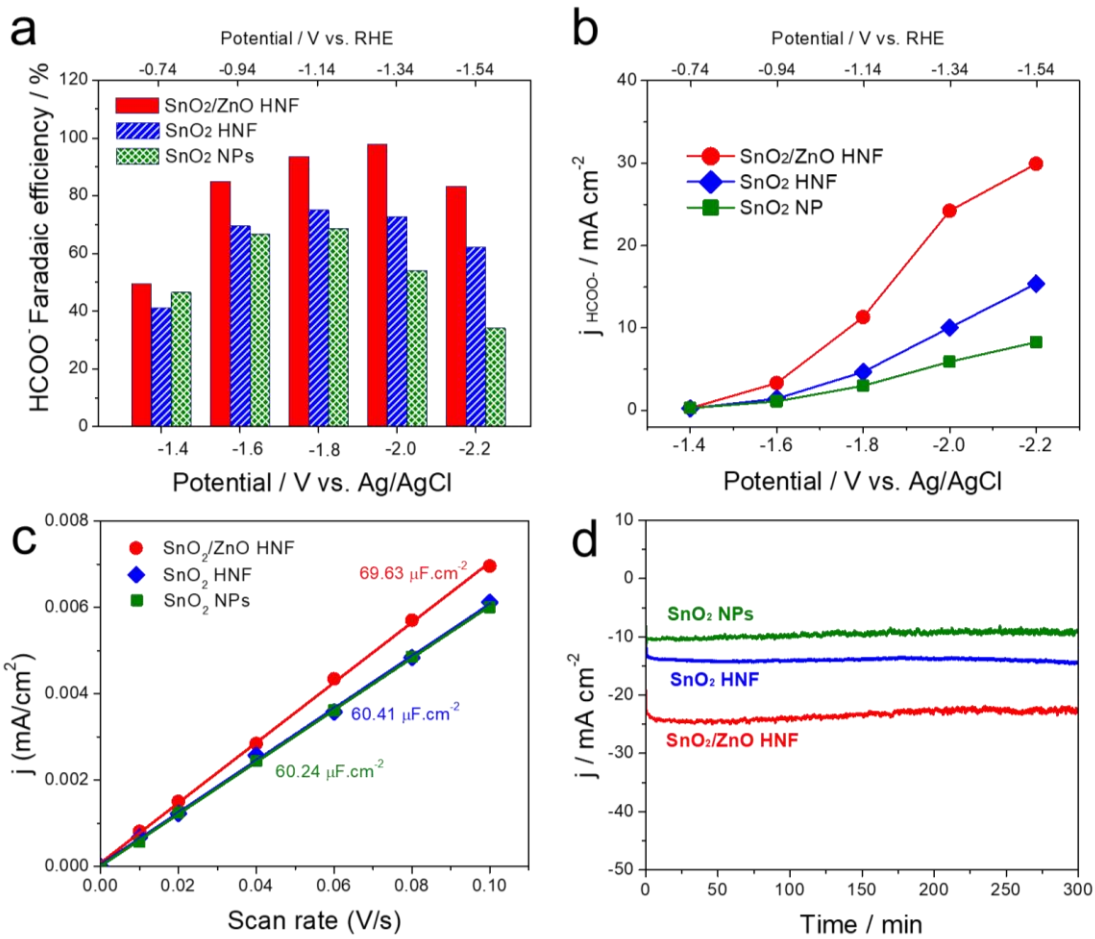

Figure 4. (**a**) Faradaic efficiency, (**b**) current density, (**c**) electrochemical surface area (ECSA), and (**d**) current stability of the SnO_2/ZnO composite HNF catalyst for formate synthesis compared with SnO_2 HNF and commercial SnO_2 nanoparticles (Reprinted with permission from reference [29]. Copyright 2020 American Chemical Society).

2.2. CO_2RR to Formate Using Gaseous CO_2 Feed

There have been experiments in CO_2 electroreduction that involve supplying gaseous CO_2 to the cathode, allowing for sufficient CO_2 delivery to the catalyst even at elevated current densities. Some research groups achieved remarkable improvement in the current density of CO_2RR to formate using gas diffusion electrodes (GDEs) typically composed of a backing layer, a microporous layer (MPL), and a catalyst layer (CL) [42–45]. Several research groups have successfully utilized GDE-type CO_2RR reactors (Figure 5a) and achieved high current densities for formate production, exceeding 200 mA cm^{-2} and even up to 1000 mA cm^{-2}, with faradaic efficiencies (FE) higher than 90% as summarized in Table 2 [46–53]. However, one challenge with GDE-type electrolyzers is that they typically use aqueous electrolytes, such as $KHCO_3$, K_2CO_3, or KOH, for the collection of liquid products. The presence of these aqueous electrolytes can dilute the liquid products, such as formate/formic acid, which increases the costs associated with product recovery and separation [54].

Table 2. Figures of merits of studies reported in the literature for the CO_2RR to formate in terms of reactor type, catalysts of the cathode, type of membrane, applied reduction potential (vs. RHE) or cell potential, faradaic efficiency, and current density for formate production.

Reactor Type	Cathode	Membrane	Cathodic Potential/Cell Voltage (V)	$FE_{formate}$ (%)	$j_{formate}$ (mA cm^{-2})	Concentration of $HCOO^-$ (wt%)	Reference
GDE-catholyte	$Bi_2O_2CO_3$ nanosheet	Fumasep FAB-PK-130	−1.55 (vs. RHE)	93	930	-	[46]
	InP colloidal quantum dots	AEM	−2.6 (vs. RHE)	93	930	-	[47]
	SnO_2 nanosheet	Selemion	−1.13 (vs. RHE)	94.2	471	-	[48]
	Pb powder	-	4	90	352	-	[49]
	Bi nanosheet	Nafion® 117	−1.18 (vs. RHE)/3.1	92.4	83.2	0.204	[51]
	$ZnIn_2S_4$ nanosheet	Nafion® 212	−1.2 (vs. RHE)	94	245	-	[52]
	Bi nanotube	Selemion	−0.56 (vs. RHE)	98	170	-	[53]
	Sn/C	Nafion® 324	−2.44 (vs. SHE)	98	200	-	[50]
Zero-gap	Bi/C	Nafion® 117	3.1	71.7	32.3	3.39	[55]
	Bi/C	Nafion® 117	3.0	89.2	40.1	33.7	[56]
	Sn nanoparticle	Nafion® 115	2.2	93.3	51.7	4.15	[54]
	Sn nanoparticle	Nafion® 115	2.2	77.7	29.8	11.62	[54]
	Bi/C	Sustainion™	3.6	91.6	274.8	0.67	[57]

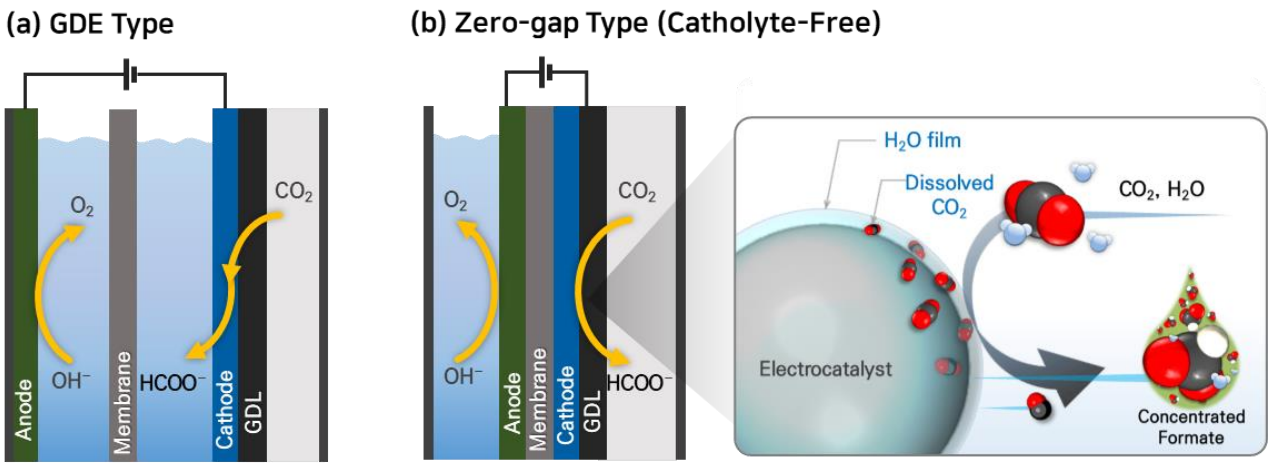

Figure 5. Electrochemical CO_2 reduction systems using gaseous CO_2 feed: (**a**) GDE-catholyte type and (**b**) zero-gap type cells.

To overcome this challenge of GDE-type reactors, some research groups have studied CO_2RR to formate in a zero-gap type electrolyzer, which eliminates the need for an aqueous electrolyte [54–57]. Lee et al. reported a facile strategy of catholyte-free electrocatalytic CO_2 reduction (CF-CO_2R) that avoids the solubility limitation by supplying an appropriate amount of water vapor with gaseous CO_2 as a cathode reactant [54]. In this electrolyzer, the water vapor. In the CF-CO_2R electrolyzer, water vapor acts as a carrier for supplying dissolved CO_2 to the cathode by forming a CO_2-saturated aqueous film on the catalyst surface as shown in Figure 5b. The advantage of this approach is that the consumed CO_2 in the film can be immediately replenished from the bulk gas stream, enhancing the mass transfer of CO_2 and improving the reaction kinetics. Lee et al. achieved a formate current density ($j_{formate}$) of 51.7 mA cm^{-2} at a low cell voltage of 2.2 V using this CF-CO_2R approach. They also obtained a significantly high concentration of formate solution, reaching 116.2 g-formate L^{-1}, with a formate faradaic efficiency ($FE_{formate}$) of 77.7% by reducing the vapor supply from 12.58 to 0.65 mg min^{-1} cm^{-2} at 2.2 V and 323 K.

The zero-gap electrolyzer has several advantages over the GDE-catholyte method, including (1) lower cell voltage and improved energy efficiency by eliminating a large ohmic resistance of the catholyte compartment; (2) reduced cost by removing the cost of the catholyte; and (3) zero-gap configuration, which makes the system simple and easy to scale up. However, the lower current density observed in this configuration is indeed due to the challenges associated with the discharge of liquid products and the formation of solid precipitates.

In the zero-gap type electrolyzer, the liquid products have to be discharged in the opposite direction of the CO_2 supply, and ions ($HCOO^-$, HCO_3^-, CO_3^{2-}, K^+, and Na^+, etc.) in the liquid products form solid precipitates, which limits the supply of CO_2. Additionally, the flow of aqueous liquid products through the gas diffusion electrode (GDE) can cause a decrease in the hydrophobicity of the electrode over time, a phenomenon known as electro-wetting. This leads to flooding of GDE that significantly inhibits the migration of CO_2 to the catalyst layer, reducing the selective reduction of CO_2 to formates while promoting the hydrogen evolution reaction (HER) as shown in Figure 6.

Recently, Díaz-Sainz et al. achieved a high $j_{formate}$ of 300 mA cm^{-2} by continuous operation using an anion exchange membrane (AEM, Sustainion^{TM}, Dioxide Materials) with a formate concentration of 6.7 g L^{-1} at a cell potential of 3.6 V [57]. In this configuration, the formate solution could be obtained at the anode because the $HCOO^-$ ions generated in the cathode are transferred to the anode side via the AEM. They even obtained higher $j_{formate}$ up to 600 mA cm^{-2} with a formate concentration of 10.8 g L^{-1} at a cell potential of 4.7 V. When AEM is used in a zero-gap type electrolyzer for formate production, the cathodic GDE flooding could be significantly reduced because $HCOO^-$ moves to the anode

through AEM, and the crossover of water and the migration of cations (K^+, Na^+, etc.) from the anode is almost completely prevented.

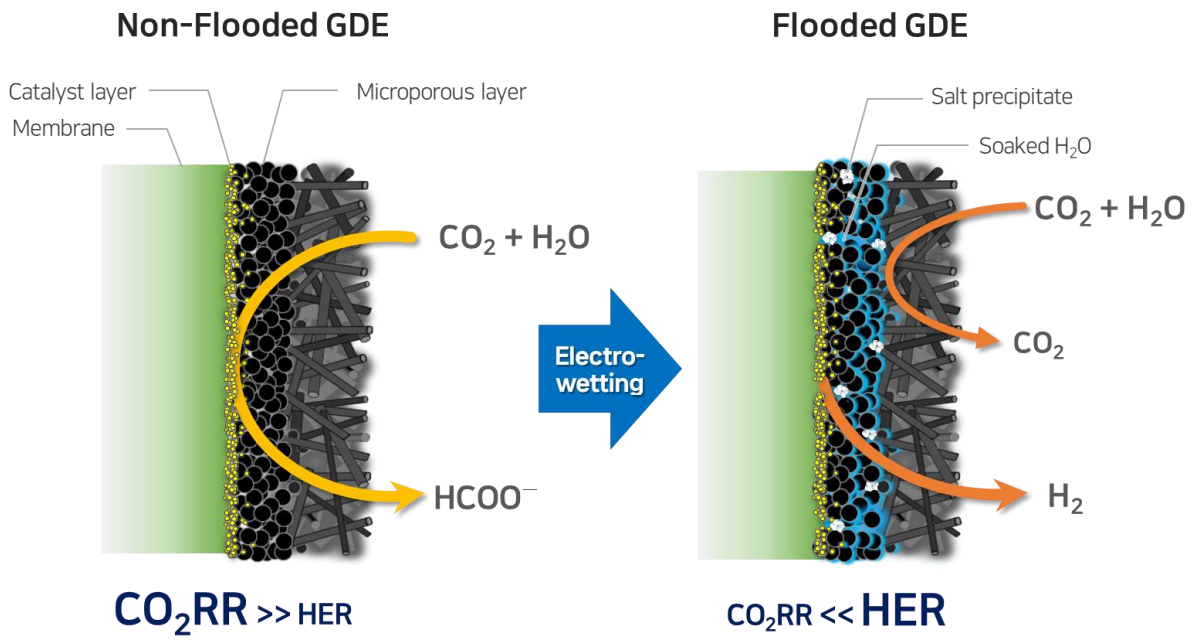

Figure 6. The schematic illustration for the problem of the GDE flooding in the zero-gap type electrolyzer by electro-wetting with electrolysis time.

3. Reactor Design for CO_2RR to Pure Formic Acid

3.1. Three-Compartment Configurations

While the research and development in GDE and zero-gap designs have resulted in remarkable advances in both faradaic efficiency and current density for formate production, these devices still have a crucial challenge to overcome. The product obtained from these reactors (GDE and zero-gap types) consists of $HCOO^-$ mixed with other impurity ions such as K^+, HCO_3^-, OH^-, and so on. This mixture is required to be separated and acidified to obtain formic acid solutions, which require a considerable amount of energy and cost [19,23,38,39,58]. Zhu et al. reported that the additional costs associated with downstream purification and concentration, which greatly affect the economic viability of liquid products. This emphasizes the necessity of achieving high-purity and high-concentration liquid products directly from CO_2 electrolyzers [37].

Therefore, the demand for technologies and devices for direct CO_2 reduction to formic acid has increased. The utilization of an additional compartment of solid-state electrolyte (SSE) in a 3-compartment reactor design presents a promising approach for the direct recovery of pure formic acid from CO_2 reduction as shown in Figure 7 [23,26,38,39]. In this design, the GDEs are employed on both the cathode and anode sides, which are in contact with an anion exchange membrane (AEM) and a cation exchange membrane (CEM), respectively. At the cathode, CO_2 reacts with water (H_2O) generating formate ($HCOO^-$) and hydroxide (OH^-) anions:

$$CO_2 + H_2O + 2e^- \rightarrow HCOO^- + OH^- \quad (1)$$

Simultaneously, the oxidation of water occurs at the anode supplied with deionized water, humidified H_2, or acidic solution, forming oxygen gas and protons (H^+):

$$2H_2O \rightarrow 4H^+ + 4e^- + O_2 \quad (2)$$

Both the $HCOO^-$ and OH^- ions migrate through the AEM into the center compartment where they meet the H^+ ions produced from the anode compartment which pass

through the CEM. In the center compartment, ionic recombination occurs, leading to the formation of HCOOH and H_2O:

$$HCOO^- + H^+ \rightarrow HCOOH \quad (3)$$

$$OH^- + H^+ \rightarrow H_2O \quad (4)$$

The produced pure HCOOH in the center compartment can be recovered by passing deionized water or a humidified N_2 stream through the porous SSE layer.

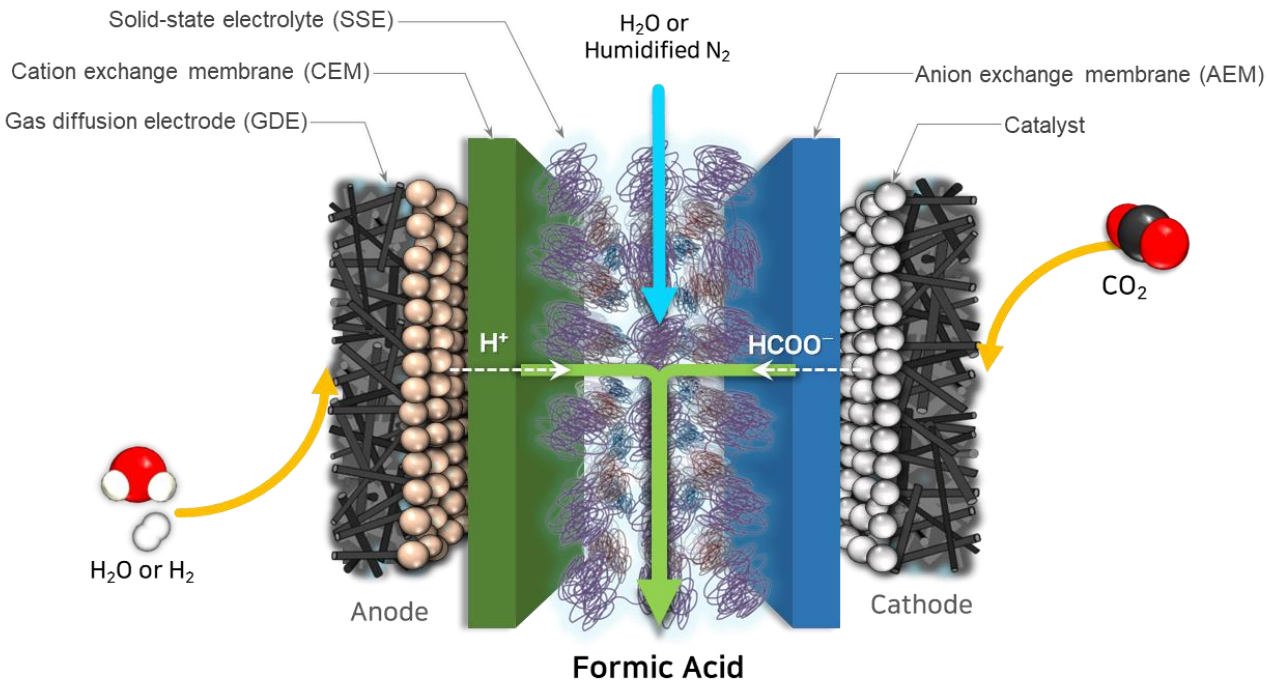

Figure 7. The schematic illustration of the electrolyzer configuration with solid-state electrolyte (SSE) to produce pure formic acid.

Side reactions that can occur on the cathode [26]:

$$CO_2 + H_2O + 2e^- \rightarrow CO + OH^- \quad (5)$$

$$2H_2O + 2e^- \rightarrow H_2 + 2OH^- \quad (6)$$

$$CO_2 + OH^- \rightarrow HCO_3^- \quad (7)$$

The bicarbonate ion (HCO_3^-) can move to the central compartment through the AEM where it reacts with protons produced on the anode to produce CO_2:

$$HCO_3^- + H^+ \rightarrow CO_2 + H_2O \quad (8)$$

Formic acid oxidation reaction that can occur on the anode [26]:

$$2HCOOH + O_2 \rightarrow 2CO_2 + 2H_2O \quad (9)$$

The 3-compartment cell design requires thin spacing in the central compartment and a high-conductivity SSE to minimize the cell IR drop. It is important to note that the conductivity of aqueous formic acid alone is relatively low, ranging between 5 and

10 mS cm^{-1} for formic acid concentrations of 5 to 20 wt% [26]. Therefore, the choice of a high-conductivity SSE is crucial to ensure efficient ionic transport and minimize energy losses within the electrolyzer system. Yang et al. investigated the ionic conductivity of four types of ion exchange resin including Amberlite® IR120, Amberlite® IRN77, Dowex® 50WX2, and Duolite C433 in water and in 5, 10, 15, and 20 wt% formic acid solutions [26]. The results of the study indicated that the use of cation ion exchange resins as SSE materials led to a significant increase in ionic conductivity compared to aqueous formic acid alone. The ion exchange resin/formic acid matrix mixtures exhibited an enhancement in ionic conductivity by a factor of approximately 6–10 compared to formic acid solutions alone. Among the SSEs tested, hydrogen-form sulfonic acid resins such as Amberlite® IR120 and Dowex® 50WX2 demonstrated high ionic conductivities. However, Dowex® 50WX2, with its fine particle size range of 100–200 mesh (75–150 µm), showed a notable pressure drop in the center flow compartment during evaluation.

3.2. Strategies for High-Purity Formic Acid Recovery

Several studies used three-compartment reactor configurations for continuous CO_2 electroreduction to recover high-purity HCOOH solution (Table 3) [23,26,38,39]. Yang et al. introduced a new approach by incorporating an acidic center compartment in their system, allowing for the direct production of formic acid instead of formate salts [26]. In this configuration, only deionized (DI) water is introduced into the center flow compartment to recover the formic acid product from the cell. The cell design included an anode compartment, a center compartment containing a cation exchange SSE enclosed by a CEM (Nafion®) on the anode side and an AEM (Sustanion™) on the cathode side, and a cathode compartment with Sn-based GDE.

The details of the configuration of their cell assembly are illustrated and summarized in Figure 8a and Table 4. They investigated the cell performances with a different flow rate of DI water in the center compartment and various ion exchange resins for the center compartment. In addition, they compared two modes of cell operation, center compartment single-pass, and recirculation modes, and found that the single-pass mode was preferred due to differences in faradaic efficiency. The study achieved a high FE_{HCOOH} of up to 94% at a current density of 140 mA cm^{-2} during 142 h or operation at a cell voltage of about 3.5 V. The HCOOH product concentration reached up to 9.4 wt% (Figure 8b). These results demonstrate the potential of the three-compartment reactor configuration for the continuous production of high-purity formic acid with improved efficiency and concentration.

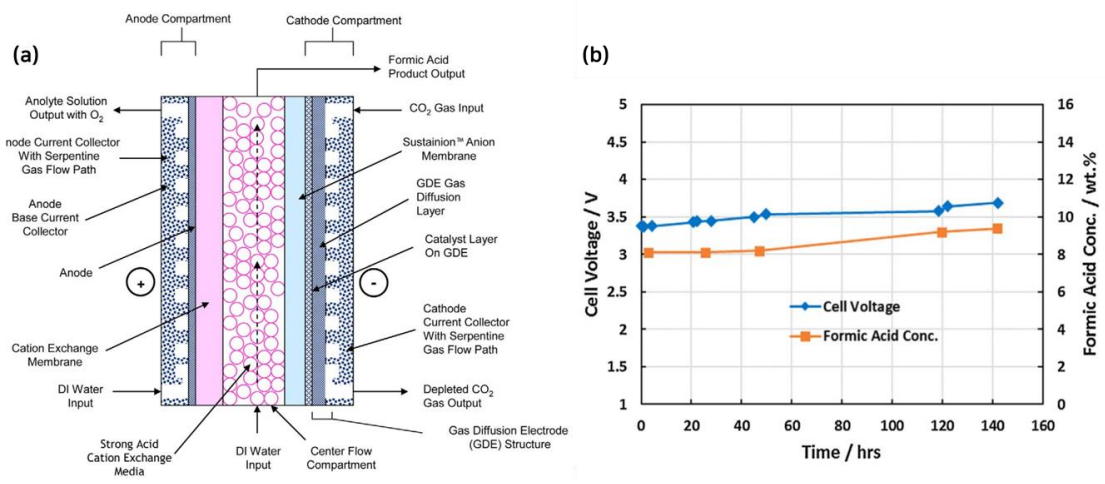

Figure 8. (**a**) The schematic illustration of 3-compartment cell configuration and (**b**) the cell performance using a titanium flow field, IrO_2 coated titanium mesh anode, and Nafion® 324 (Reprinted with permission from reference [26]. Copyright 2017 Elsevier).

Table 3. Figures of merits of studies reported in the literature for the CO_2RR to pure formic acid in terms of catalysts of the cathode, type of membranes, the material of SSE, type of feeds for cathode, anode, and SSE, applied cell voltage, faradaic efficiency, current density, and concentration of formic acid.

Cathode	Membrane (AEM/CEM)	SSE Material	Feeds		Cell Voltage (V)	FE_{HCOOH} (%)	j_{HCOOH} (mA cm^{-2})	Concentration of HCOOH (wt%)	Reference
			Cathode/Anode	SSE					
Sn	Sustanion/ Nafion® 324	Amberlite® IR120	Humidified-CO_2/H_2O	H_2O	3.5	94	131.6	9.4	[26]
2D-Bi	Sustanion/ Nafion® 115	SVB copolymer	Humidified-CO_2/H_2O Humidified-CO_2/H_2O Humidified-CO_2/ Humidified-H_2	H_2O Humidified-N_2 Humidified-N_2	3.08 2.75 1.33	93.1 40 73.3	32.1 80 163	0.51 49.3 -	[38]
Bi	PSMIM/ Nafion® 115	SVB copolymer	Humidified-CO_2/ Humidified-H_2	H_2O Humidified-N_2 Dry N_2	2.19 1.49 -	97 40 ~22	450 80 44	~3 11 ~100	[23]
Bi_2O_3	Sustanion/ Nafion® 324	Amberlite® IR120	Humidified-CO_2/H_2O	H_2O	3.76	91.3	182.6	6.03	[39]

Table 4. Formic acid cell assembly configuration summary of Yang et al. group (Reprinted with permission from reference [26]. Copyright 2017 Elsevier).

Cathode configurations	Cathode	POCO Graphite block with the serpentine flow path
	GDE cathode	Toray paper, 50% PTFE proofing
	GDE catalyst	Sn nanoparticles (99.9%, 60–80 nm, US Research Nanomaterials, Inc.), catalyst layer air atomized onto GDE cathode with varying amounts of PTFE suspension and 5% imidazolium-based ionomer, and 5% carbon nanotubes.
	CO_2 flowrate	20 mL/min, not humidified for ambient temperature operation
Anode configurations	Anode 1	POCO Graphite block with the serpentine flow path. The anode was a GDE electrode with a 2 mg cm^{-2} IrO_2 catalyst (99.99%, Alfa Aesar) onto 5% PTFE proofing Toray paper
	Anode 2	Titanium Grade 2 anode block with the serpentine flow path. The Anode screen having IrO_2-based metal oxide coating on expanded titanium (Water Star) was spot welded onto the titanium anode block
	Anolyte recirculation rate	DI water, 8–12 mL/min
Center flow compartment	Ion exchange media	Amberlite® IR120 strong acid ion exchange resin fill, 620–830 µm beads, and other selected ion exchange resins
	Center compartment	1 mm thickness, 2.25 cm × 2.25 cm, 0.50 mL (empty), estimated 40% void volume, i.e., 0.2 mL free volume with ion exchange resin
	Center compartment frame	Polycarbonate, the machined flow path for solution flow in/out
	DI water feed	Selected rate of 0.03 1 mL/min into center flow compartment
Anion membrane		Dioxide Materials Sustainion™ X37 imidazolium-based anion exchange membrane:60–80 µm thickness (wet), ion exchange capacity of 1.05 mEq/g (950 EW), membrane conductivity in water, through the plane, of about 60–70 mS cm^{-1}
Cation membranes		DuPont Nafion® Membranes Tested: 212, 115, 324
Active geometric area		5 cm^2
Cell operating temperature		Ambient, 20–25 °C

Yang et al. also demonstrated the long-term stability of pure formic acid production by 1000 h operation of the 3-compartment design at industrially relevant current densities [39]. The electrolyzer (Figure 9a) can be operated at a current density as high as 300 mA cm^{-2} with a cell voltage below 4.0 V, and no significant change in FE_{HCOOH} was observed at current densities between 100 and 250 mA cm^{-2}. Typically, higher DI water flow rates led to higher FE_{HCOOH} but lower HCOOH concentrations as shown in Figure 9b. The electrolyzer directly produced a 6.03–12.92 wt% formic acid product at FE_{HCOOH} range of 73.0–91.3%, depending on the operating conditions. The highest formic acid FE of 91.3% was achieved using a center compartment DI water flow rate of 0.17 mL min^{-1} with an HCOOH concentration of 6.03 wt%. In addition, they confirmed that the FE $_{HCOOH}$ was mostly above 70% and HCOOH concentration above 11 wt% during the 1000 h long-term test at 200 mA cm^{-2} (Figure 9c).

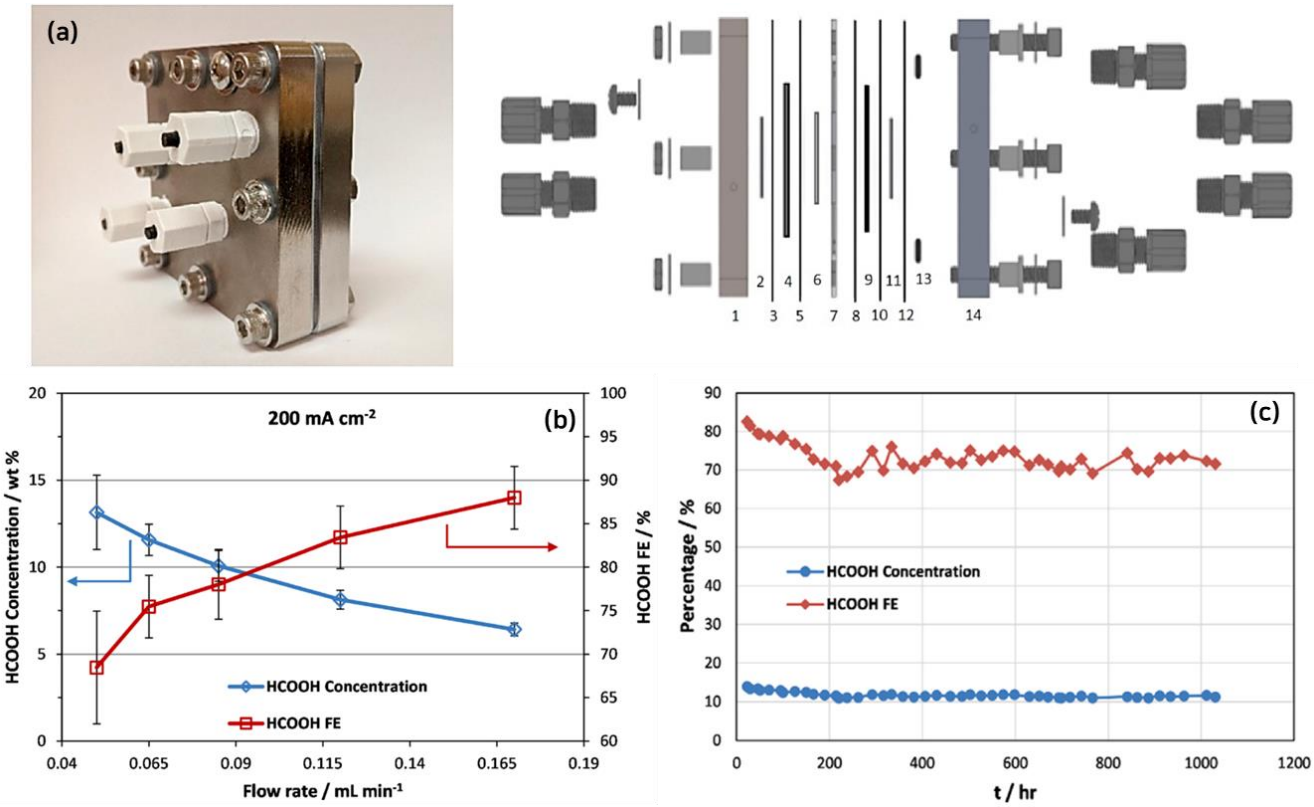

Figure 9. (**a**) A photo of an assembled electrolyzer (**left**) and the exploded view (**right**) (1: cathode flow field and current collector; 2: cathode GDE; 3, 5, 8, 10, 12: PTFE gaskets; 4: anion exchange membrane; 6: ion exchange media; 7: center compartment; 9: cation exchange membrane; 11: anode GDE; 13: O-rings; 14: anode flow field and current collector); (**b**) the HCOOH concentration and FE_{HCOOH} as a function of the center compartment DI water flow rate; and (**c**) the HCOOH concentration and FE_{HCOOH} during 1000 h operation (Reprinted with permission from reference [39]. Copyright 2020 Elsevier).

Xia and Wang's group also demonstrated the production of high-purity formic acid using the 3-compartment cell design using an ultrathin two-dimensional Bi (2D-Bi) catalyst for CO_2RR to HCOOH [38]. They used a porous styrene–divinylbenzene (SVB) copolymer as SSE consisting of sulfonic acid functional groups for H^+ conduction. They obtained a 0.112 M (~0.5 wt%) pure HCOOH solution with a peak FE_{HCOOH} of 93.1% and a partial current density of 32.1 mA cm^{-2} at 3.08 V and at a DI water flowrate into the center compartment of 12 mL h^{-1}.

However, they pointed out a few challenges that remain impeding its practical applications: (i) the concentration of the product was limited due to the use of DI water in the

SSE layer; (ii) the rate of product generation was not sufficiently high to meet the demands of industrial applications; (iii) the system still relied on the use of a liquid electrolyte on the anode side for water oxidation [23]. To achieve a high concentration of formic acid solutions, it is necessary to reduce the flow rate of DI water. However, it should be noted that increasing the concentration of formic acid in the SSE layer can lead to a significant decrease in faradaic efficiency. This is because higher formic acid concentrations can increase the rate of the reverse reaction and result in increased crossover to the anode. In this concern, they suggested an all-solid-state reactor, where an inert gas (N_2) flow is supplied to recover high-purity HCOOH vapor from the center compartment instead of DI water. High-purity HCOOH can be obtained by a simple cold condensation process. As a result, they accomplished HCOOH concentration up to 12.1 M (~49.3 wt%) using 10 sccm of humidified N_2 gas [38], and nearly 100 wt% pure HCOOH using 20 sccm of dry N_2 gas [23] instead of DI water flow to recover the generated HCOOH. This alternative approach of utilizing an all-solid-state reactor with N_2 gas flow offers several advantages. It enables higher formic acid concentrations without sacrificing faradaic efficiency, as the dilution effect from DI water is eliminated. Additionally, the recovery of high-purity formic acid vapor through a cold condensation process simplifies the product separation step.

3.3. Opportunities and Challenges

The 3-compartment electrolyzer design using SSE offers a promising pathway for the direct production of high-purity formic acid (HCOOH) and represents a significant step towards commercializing CO2RR technologies. One key advantage of the SSE reactor design is its ability to prevent the crossover of cathode-generated carbonate ions [59]. In the typical 2-compartment electrolyzer, hydroxide ions (OH^-) generated at the cathode during CO_2RR react rapidly with the supplied CO_2 to form carbonate (CO_3^{2-}) or bicarbonate (HCO_3^-) ions, which move across the AEM to the anodic side, resulting in carbon loss. On the other hand, in the SSE reactor design, the CO_3^{2-} or HCO_3^- ions migrate through AEM into the center compartment and then be recombined with protons from the anode to form CO_2 gas again, which could be easily recirculated to the cathodic reactant.

While the SSE approach offers advantages in terms of product separation energy and cost, it introduces the challenge of increased ohmic resistance, which can reduce the energy efficiency of CO_2RR. Thus, the energy penalty by increased ohmic resistance should be compared with the energy required to separate the liquid fuels from the electrolyte. It is possible to reduce the resistance of the solid-state electrolyte (SSE) by engineering ultra-thin SSE layers [38]. This can be achieved by decreasing the thickness of the SSE, which would enhance the ion conductivity within the solid electrolyte. Additionally, improving the contact interface between the SSE layer and the membranes can also contribute to reducing resistance [37]. Beyond the conventional formate production technology, there was remarkable progress in high-purity formic acid production via adopting a 3-compartment electrolyzer using SSE, which exhibited nearly 100 wt% pure formic acid. However, it is important to note that high-purity formic acid has not yet been produced at commercially relevant partial current densities (>200 mA cm^{-2}). This highlights the need for further research and development efforts to optimize the SSE reactor design, enhance the current density, and improve the energy efficiency to make high-purity formic acid production economically viable at larger scales. Figure 10 illustrates the current status of high-purity formic acid production, indicating that there is still room for improvement in achieving commercially relevant partial current densities while maintaining high purity. Future research should aim to overcome these challenges and explore innovative strategies to enhance the performance and scalability of the SSE-based 3-compartment electrolyzer for efficient and commercially viable formic acid production.

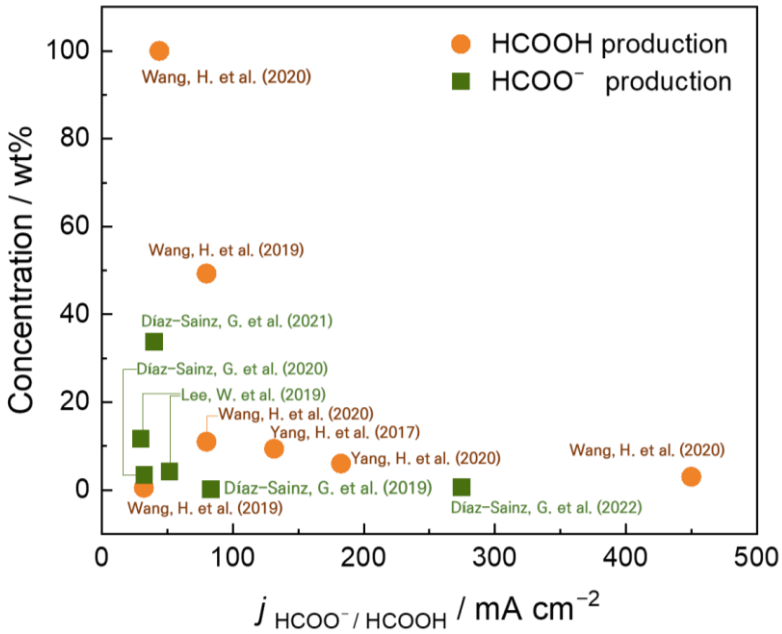

Figure 10. Comparison of the concentration of formate ($HCOO^-$) and formic acid (HCOOH) products reported in the literature via CO_2RR from GDE, zero-gap, and 3-compartment reactors as a function of partial current density [23,26,38,39,51,54–57].

4. Summary and Outlooks

In summary, recent research has been reviewed in reactor design for formic acid production to address the challenges of impurity and low concentration in conventional CO_2RR reactors. Early studies focused on producing formate in aqueous solutions using 3-electrode and H-type cells. However, the limited solubility of CO_2 in the aqueous catholyte restricted the current density and hindered the large-scale application of CO_2RR. To overcome this limitation, researchers have introduced reactor designs that ensure sufficient CO_2 supply to the catalyst. GDE-type reactors and zero-gap electrolyzers have shown significant improvements in formate current density, reaching up to 930 mA cm^{-2}, and achieving concentrated formate products of up to 33.7 wt%. However, these products contain impurity ions, requiring downstream processes such as separation and acidification to obtain pure formic acid. One promising approach to obtaining pure formic acid is the incorporation of an additional SSE compartment between the anode and cathode. This 3-compartment electrolyzer has demonstrated the production of nearly 100 wt% pure formic acid. However, high-purity formic acid has not yet been produced at commercially relevant partial current densities.

Future research should focus on developing cost-effective and scalable technologies for formic acid production from CO_2RR. This includes exploring catalyst materials that are abundant, low-cost, and highly efficient. Additionally, optimizing reactor designs and process parameters to maximize productivity and minimize energy consumption will be crucial for cost-effective large-scale production. To enhance the economic viability of the liquid products, it is crucial to achieve high-purity and high-concentration formic acid directly from the CO_2 electrolyzer. This would eliminate or minimize the need for extensive downstream processing, reducing energy consumption, operational costs, and capital investments associated with purification and concentration steps. Future progress in this approach also provides a potential route to store H_2 in liquid HCOOH and could be extended to the production of C_{2+} liquid fuels. This review contributes to the advancement of electrolyzer technology, bringing us closer to large-scale applications of CO_2RR for the production of high-purity formic acid and other liquid fuels in the future.

Author Contributions: Conceptualization, K.T.P. and Y.K.; investigation, K.T.P., Y.K., T.K. and K.Y.J.; data curation, Y.K., T.K. and K.Y.J.; writing—original draft preparation, K.T.P. and Y.K.; writing—review and editing, K.T.P. and Y.K.; visualization, K.T.P.; supervision, K.T.P.; funding acquisition, K.T.P. All authors have read and agreed to the published version of the manuscript.

Funding: This research was funded by Konkuk University (2022-A019-0009).

Data Availability Statement: The data presented in this study are available in the corresponding references listed.

Acknowledgments: This paper was supported by Konkuk University in 2023.

Conflicts of Interest: The authors declare no conflict of interest.

References

1. Duarah, P.; Haldar, D.; Yadav, V.S.K.; Purkait, M.K. Progress in the electrochemical reduction of CO_2 to formic acid: A review on current trends and future prospects. *J. Environ. Chem. Eng.* **2021**, *9*, 106394. [CrossRef]
2. Zarandi, R.F.; Rezaei, B.; Ghaziaskar, H.S.; Ensafi, A.A. Electrochemical reduction of CO_2 to ethanol using copper nanofoam electrode and 1-butyl-3-methyl-imidazolium bromide as the homogeneous co-catalyst. *J. Environ. Chem. Eng.* **2019**, *7*, 103141. [CrossRef]
3. Jeon, Y.E.; Ko, Y.N.; Kim, J.; Choi, H.; Lee, W.; Kim, Y.E.; Lee, D.; Kim, H.Y.; Park, K.T. Selective production of ethylene from CO_2 over CuAg tandem electrocatalysts. *J. Ind. Eng. Chem.* **2022**, *116*, 191–198. [CrossRef]
4. Salimijazi, F.; Kim, J.; Schmitz, A.M.; Grenville, R.; Bocarsly, A.; Barstow, B. Constraints on the Efficiency of Engineered Electromicrobial Production. *Joule* **2020**, *4*, 2101–2130. [CrossRef]
5. Gunasekar, G.H.; Park, K.; Jung, K.-D.; Yoon, S. Recent developments in the catalytic hydrogenation of CO_2 to formic acid/formate using heterogeneous catalysts. *Inorg. Chem. Front.* **2016**, *3*, 882–895. [CrossRef]
6. Ma, Z.; Wan, T.; Zhang, D.; Yuwono, J.A.; Tsounis, C.; Jiang, J.; Chou, Y.-H.; Lu, X.; Kumar, P.V.; Ng, Y.H.; et al. Atomically Dispersed Cu Catalysts on Sulfide-Derived Defective Ag Nanowires for Electrochemical CO_2 Reduction. *ACS Nano* **2023**, *17*, 2387–2398. [CrossRef]
7. Jouny, M.; Luc, W.; Jiao, F. General Techno-Economic Analysis of CO_2 Electrolysis Systems. *Ind. Eng. Chem. Res.* **2018**, *57*, 2165–2177. [CrossRef]
8. Gu, J.; Hsu, C.-S.; Bai, L.; Chen, H.M.; Hu, X. Atomically dispersed Fe3+ sites catalyze efficient CO_2 electroreduction to CO. *Science* **2019**, *364*, 1091–1094. [CrossRef]
9. Zheng, T.; Jiang, K.; Ta, N.; Hu, Y.; Zeng, J.; Liu, J.; Wang, H. Large-Scale and Highly Selective CO_2 Electrocatalytic Reduction on Nickel Single-Atom Catalyst. *Joule* **2019**, *3*, 265–278. [CrossRef]
10. Higgins, D.; Hahn, C.; Xiang, C.; Jaramillo, T.F.; Weber, A.Z. Gas-Diffusion Electrodes for Carbon Dioxide Reduction: A New Paradigm. *ACS Energy Lett.* **2018**, *4*, 317–324. [CrossRef]
11. Lee, J.; Lee, W.; Ryu, K.H.; Park, J.; Lee, H.; Lee, J.H.; Park, K.T. Catholyte-free electroreduction of CO_2 for sustainable production of CO: Concept, process development, techno-economic analysis, and CO_2 reduction assessment. *Green Chem.* **2021**, *23*, 2397–2410. [CrossRef]
12. Lee, S.; Eun Jeon, Y.; Lee, S.; Lee, W.; Kim, S.; Choi, J.; Park, J.; Woo Han, J.; Na Ko, Y.; Eun Kim, Y.; et al. Deciphering Mass Transport Behavior in Membrane Electrode Assembly by Manipulating Porous Structures of Atomically Dispersed Metal-Nx Catalysts for High-Efficiency Electrochemical CO_2 Conversion. *Chem. Eng. J.* **2023**, *464*, 142593. [CrossRef]
13. Eppinger, J.; Huang, K.-W. Formic Acid as a Hydrogen Energy Carrier. *ACS Energy Lett.* **2016**, *2*, 188–195. [CrossRef]
14. Wang, L.; Nitopi, S.; Wong, A.B.; Snider, J.L.; Nielander, A.C.; Morales-Guio, C.G.; Orazov, M.; Higgins, D.C.; Hahn, C.; Jaramillo, T.F. Electrochemically converting carbon monoxide to liquid fuels by directing selectivity with electrode surface area. *Nat. Catal.* **2019**, *2*, 702–708. [CrossRef]
15. Mardini, N.; Bicer, Y. Direct synthesis of formic acid as hydrogen carrier from CO_2 for cleaner power generation through direct formic acid fuel cell. *Int. J. Hydrog. Energy* **2021**, *46*, 13050–13060. [CrossRef]
16. Moret, S.; Dyson, P.J.; Laurenczy, G. Direct synthesis of formic acid from carbon dioxide by hydrogenation in acidic media. *Nat. Commun.* **2014**, *5*, 4017. [CrossRef]
17. Wang, W.-H.; Himeda, Y.; Muckerman, J.T.; Manbeck, G.F.; Fujita, E. CO_2 Hydrogenation to Formate and Methanol as an Alternative to Photo- and Electrochemical CO_2 Reduction. *Chem. Rev.* **2015**, *115*, 12936–12973. [CrossRef]
18. Álvarez, A.; Bansode, A.; Urakawa, A.; Bavykina, A.V.; Wezendonk, T.A.; Makkee, M.; Gascon, J.; Kapteijn, F. Challenges in the Greener Production of Formates/Formic Acid, Methanol, and DME by Heterogeneously Catalyzed CO_2Hydrogenation Processes. *Chem. Rev.* **2017**, *117*, 9804–9838. [CrossRef]
19. Orella, M.J.; Brown, S.M.; Leonard, M.E.; Román-Leshkov, Y.; Brushett, F.R. A General Technoeconomic Model for Evaluating Emerging Electrolytic Processes. *Energy Technol.* **2019**, *8*, 1900994. [CrossRef]
20. Mellmann, D.; Sponholz, P.; Junge, H.; Beller, M. Formic acid as a hydrogen storage material—Development of homogeneous catalysts for selective hydrogen release. *Chem. Soc. Rev.* **2016**, *45*, 3954–3988. [CrossRef]

21. Liu, L.-X.; Zhou, Y.; Chang, Y.-C.; Zhang, J.-R.; Jiang, L.-P.; Zhu, W.; Lin, Y. Tuning Sn3O4 for CO_2 reduction to formate with ultra-high current density. *Nano Energy* **2020**, *77*, 105296. [CrossRef]
22. Kumar, B.; Atla, V.; Brian, J.P.; Kumari, S.; Nguyen, T.Q.; Sunkara, M.; Spurgeon, J.M. Reduced SnO_2 Porous Nanowires with a High Density of Grain Boundaries as Catalysts for Efficient Electrochemical CO_2-into-COOH Conversion. *Angew. Chem. Int. Ed. Engl.* **2017**, *56*, 3645–3649. [CrossRef] [PubMed]
23. Fan, L.; Xia, C.; Zhu, P.; Lu, Y.; Wang, H. Electrochemical CO(2) reduction to high-concentration pure formic acid solutions in an all-solid-state reactor. *Nat. Commun.* **2020**, *11*, 3633. [CrossRef]
24. Liang, X.-D.; Tian, N.; Hu, S.-N.; Zhou, Z.-Y.; Sun, S.-G. Recent advances of bismuth-based electrocatalysts for CO_2 reduction: Strategies, mechanism and applications. *Mater. Rep. Energy* **2023**, *3*, 100191. [CrossRef]
25. Shin, H.; Hansen, K.U.; Jiao, F. Techno-economic assessment of low-temperature carbon dioxide electrolysis. *Nat. Sustain.* **2021**, *4*, 911–919. [CrossRef]
26. Yang, H.; Kaczur, J.J.; Sajjad, S.D.; Masel, R.I. Electrochemical conversion of CO_2 to formic acid utilizing Sustainion™ membranes. *J. CO2 Util.* **2017**, *20*, 208–217. [CrossRef]
27. Choi, S.Y.; Jeong, S.K.; Kim, H.J.; Baek, I.-H.; Park, K.T. Electrochemical Reduction of Carbon Dioxide to Formate on Tin–Lead Alloys. *ACS Sustain. Chem. Eng.* **2016**, *4*, 1311–1318. [CrossRef]
28. Kim, Y.E.; Lee, W.; Ko, Y.N.; Park, J.E.; Tan, D.; Hong, J.; Jeon, Y.E.; Oh, J.; Park, K.T. Role of Binder in Cu2O Gas Diffusion Electrodes for CO_2 Reduction to C2+ Products. *ACS Sustain. Chem. Eng.* **2022**, *10*, 11710–11718. [CrossRef]
29. Tan, D.; Lee, W.; Kim, Y.E.; Ko, Y.N.; Youn, M.H.; Jeon, Y.E.; Hong, J.; Jeong, S.K.; Park, K.T. SnO_2/ZnO Composite Hollow Nanofiber Electrocatalyst for Efficient CO_2 Reduction to Formate. *ACS Sustain. Chem. Eng.* **2020**, *8*, 10639–10645. [CrossRef]
30. Tan, D.; Lee, W.; Kim, Y.E.; Ko, Y.N.; Youn, M.H.; Jeon, Y.E.; Hong, J.; Park, J.E.; Seo, J.; Jeong, S.K.; et al. In-Bi Electrocatalyst for the Reduction of CO(2) to Formate in a Wide Potential Window. *ACS Appl. Mater. Interfaces* **2022**, *14*, 28890–28899. [CrossRef]
31. Tan, D.; Lee, W.; Park, K.T.; Jeon, Y.E.; Hong, J.; Ko, Y.N.; Kim, Y.E. Promoting CO_2 reduction to formate selectivity on indium-doped tin oxide nanowires. *Appl. Surf. Sci.* **2023**, *613*, 155944. [CrossRef]
32. Hu, H.; Gui, L.; Zhou, W.; Sun, J.; Xu, J.; Wang, Q.; He, B.; Zhao, L. Partially reduced Sn/SnO_2 porous hollow fiber: A highly selective, efficient and robust electrocatalyst towards carbon dioxide reduction. *Electrochim. Acta* **2018**, *285*, 70–77. [CrossRef]
33. Lv, W.; Zhou, J.; Bei, J.; Zhang, R.; Wang, L.; Xu, Q.; Wang, W. Electrodeposition of nano-sized bismuth on copper foil as electrocatalyst for reduction of CO_2 to formate. *Appl. Surf. Sci.* **2017**, *393*, 191–196. [CrossRef]
34. Wu, Z.; Wu, H.; Cai, W.; Wen, Z.; Jia, B.; Wang, L.; Jin, W.; Ma, T. Engineering Bismuth–Tin Interface in Bimetallic Aerogel with a 3D Porous Structure for Highly Selective Electrocatalytic CO_2 Reduction to HCOOH. *Angew. Chem.* **2021**, *133*, 12662–12667. [CrossRef]
35. Bai, X.; Chen, W.; Zhao, C.; Li, S.; Song, Y.; Ge, R.; Wei, W.; Sun, Y. Exclusive Formation of Formic Acid from CO_2 Electroreduction by a Tunable Pd-Sn Alloy. *Angew. Chem.* **2017**, *129*, 12387–12391. [CrossRef]
36. Luc, W.; Collins, C.; Wang, S.; Xin, H.; He, K.; Kang, Y.; Jiao, F. Ag–Sn Bimetallic Catalyst with a Core–Shell Structure for CO_2 Reduction. *J. Am. Chem. Soc.* **2017**, *139*, 1885–1893. [CrossRef]
37. Zhu, P.; Wang, H. High-purity and high-concentration liquid fuels through CO_2 electroreduction. *Nat. Catal.* **2021**, *4*, 943–951. [CrossRef]
38. Xia, C.; Zhu, P.; Jiang, Q.; Pan, Y.; Liang, W.; Stavitski, E.; Alshareef, H.N.; Wang, H. Continuous production of pure liquid fuel solutions via electrocatalytic CO_2 reduction using solid-electrolyte devices. *Nat. Energy* **2019**, *4*, 776–785. [CrossRef]
39. Yang, H.; Kaczur, J.J.; Sajjad, S.D.; Masel, R.I. Performance and long-term stability of CO_2 conversion to formic acid using a three-compartment electrolyzer design. *J. CO2 Util.* **2020**, *42*, 101349. [CrossRef]
40. Daiyan, R.; Lu, X.; Saputera, W.H.; Ng, Y.H.; Amal, R. Highly Selective Reduction of CO_2 to Formate at Low Overpotentials Achieved by a Mesoporous Tin Oxide Electrocatalyst. *ACS Sustain. Chem. Eng.* **2018**, *6*, 1670–1679. [CrossRef]
41. Hori, Y. Electrochemical CO2 Reduction on Metal Electrodes. In *Modern Aspects of Electrochemistry*; Springer: New York, NY, USA, 2008; pp. 89–189. [CrossRef]
42. Song, J.; Song, H.; Kim, B.; Oh, J. Towards Higher Rate Electrochemical CO_2 Conversion: From Liquid-Phase to Gas-Phase Systems. *Catalysts* **2019**, *9*, 224. [CrossRef]
43. Verma, S.; Lu, X.; Ma, S.; Masel, R.I.; Kenis, P.J.A. The effect of electrolyte composition on the electroreduction of CO_2 to CO on Ag based gas diffusion electrodes. *Phys. Chem. Chem. Phys.* **2016**, *18*, 7075–7084. [CrossRef] [PubMed]
44. Kutz, R.B.; Chen, Q.; Yang, H.; Sajjad, S.D.; Liu, Z.; Masel, I.R. Sustainion Imidazolium-Functionalized Polymers for Carbon Dioxide Electrolysis. *Energy Technol.* **2017**, *5*, 929–936. [CrossRef]
45. Dinh, C.-T.; García de Arquer, F.P.; Sinton, D.; Sargent, E.H. High Rate, Selective, and Stable Electroreduction of CO_2 to CO in Basic and Neutral Media. *ACS Energy Lett.* **2018**, *3*, 2835–2840. [CrossRef]
46. Fan, T.; Ma, W.; Xie, M.; Liu, H.; Zhang, J.; Yang, S.; Huang, P.; Dong, Y.; Chen, Z.; Yi, X. Achieving high current density for electrocatalytic reduction of CO_2 to formate on bismuth-based catalysts. *Cell Rep. Phys. Sci.* **2021**, *2*, 100353. [CrossRef]
47. Grigioni, I.; Sagar, L.K.; Li, Y.C.; Lee, G.; Yan, Y.; Bertens, K.; Miao, R.K.; Wang, X.; Abed, J.; Won, D.H.; et al. CO_2 Electroreduction to Formate at a Partial Current Density of 930 mA cm–2 with InP Colloidal Quantum Dot Derived Catalysts. *ACS Energy Lett.* **2020**, *6*, 79–84. [CrossRef]
48. Li, J.; Jiao, J.; Zhang, H.; Zhu, P.; Ma, H.; Chen, C.; Xiao, H.; Lu, Q. Two-Dimensional SnO_2 Nanosheets for Efficient Carbon Dioxide Electroreduction to Formate. *ACS Sustain. Chem. Eng.* **2020**, *8*, 4975–4982. [CrossRef]

49. Lu, X.; Leung, D.Y.C.; Wang, H.; Xuan, J. A high performance dual electrolyte microfluidic reactor for the utilization of CO_2. *Appl. Energy* **2017**, *194*, 549–559. [CrossRef]
50. Pavesi, D.; van de Poll, R.C.J.; Krasovic, J.L.; Figueiredo, M.; Gruter, G.-J.M.; Koper, M.T.M.; Schouten, K.J.P. Cathodic Disintegration as an Easily Scalable Method for the Production of Sn- and Pb-Based Catalysts for CO_2 Reduction. *ACS Sustain. Chem. Eng.* **2020**, *8*, 15603–15610. [CrossRef]
51. Díaz-Sainz, G.; Alvarez-Guerra, M.; Solla-Gullón, J.; García-Cruz, L.; Montiel, V.; Irabien, A. CO_2 electroreduction to formate: Continuous single-pass operation in a filter-press reactor at high current densities using Bi gas diffusion electrodes. *J. CO2 Util.* **2019**, *34*, 12–19. [CrossRef]
52. Wang, Z.; Qi, R.; Liu, D.; Zhao, X.; Huang, L.; Chen, S.; Chen, Z.; Li, M.; You, B.; Pang, Y.; et al. Exfoliated Ultrathin ZnIn(2) S(4) Nanosheets with Abundant Zinc Vacancies for Enhanced CO(2) Electroreduction to Formate. *ChemSusChem* **2021**, *14*, 852–859. [CrossRef]
53. Gong, Q.; Ding, P.; Xu, M.; Zhu, X.; Wang, M.; Deng, J.; Ma, Q.; Han, N.; Zhu, Y.; Lu, J.; et al. Structural defects on converted bismuth oxide nanotubes enable highly active electrocatalysis of carbon dioxide reduction. *Nat. Commun.* **2019**, *10*, 2807. [CrossRef]
54. Lee, W.; Kim, Y.E.; Youn, M.H.; Jeong, S.K.; Park, K.T. Catholyte-Free Electrocatalytic CO_2 Reduction to Formate. *Angew. Chem. Int. Ed. Engl.* **2018**, *57*, 6883–6887. [CrossRef]
55. Díaz-Sainz, G.; Alvarez-Guerra, M.; Solla-Gullón, J.; García-Cruz, L.; Montiel, V.; Irabien, A. Gas–liquid–solid reaction system for CO_2 electroreduction to formate without using supporting electrolyte. *AIChE J.* **2020**, *66*, e16299. [CrossRef]
56. Díaz-Sainz, G.; Alvarez-Guerra, M.; Ávila-Bolívar, B.; Solla-Gullón, J.; Montiel, V.; Irabien, A. Improving trade-offs in the figures of merit of gas-phase single-pass continuous CO_2 electrocatalytic reduction to formate. *Chem. Eng. J.* **2021**, *405*, 126965. [CrossRef]
57. Díaz-Sainz, G.; Alvarez-Guerra, M.; Irabien, A. Continuous electroreduction of CO_2 towards formate in gas-phase operation at high current densities with an anion exchange membrane. *J. CO2 Util.* **2022**, *56*, 101822. [CrossRef]
58. Bushuyev, O.S.; De Luna, P.; Dinh, C.T.; Tao, L.; Saur, G.; van de Lagemaat, J.; Kelley, S.O.; Sargent, E.H. What Should We Make with CO_2 and How Can We Make It? *Joule* **2018**, *2*, 825–832. [CrossRef]
59. Xing, Z.; Hu, L.; Ripatti, D.S.; Hu, X.; Feng, X. Enhancing carbon dioxide gas-diffusion electrolysis by creating a hydrophobic catalyst microenvironment. *Nat. Commun.* **2021**, *12*, 136. [CrossRef]